Palaeogeography, Palaeoclimatology, Palaeoecology 495 (2018) 214–226

Contents lists available at ScienceDirect

Palaeogeography, Palaeoclimatology, Palaeoecology

journal homepage: www.elsevier.com/locate/palaeo

Climate forcings on vegetation of the southeastern Yucatán Peninsula (Mexico) during the middle to late Holocene

Alejandro A. Aragón-Moreno[a], Gerald A. Islebe[a,*], Priyadarsi D. Roy[b], Nuria Torrescano-Valle[a], Andreas D. Mueller[c]

[a] El Colegio de la Frontera Sur, AP 424, CP 77000 Chetumal, Quintana Roo, Mexico
[b] Instituto de Geología, Universidad Nacional Autónoma de México, Ciudad Universitaria, CP 04510 Ciudad de Mexico, Mexico
[c] ETH-Library, Subject Specialist Geosciences & Curator a.i. Geological-Palaeontological Collection, Rämistrasse 101, 8092 Zürich, Switzerland

ARTICLE INFO

Keywords:
ENSO
ITCZ
Vegetation response
Geochemistry
Caribbean
Fossil pollen

ABSTRACT

Climate and vegetation history from the Yucatán Peninsula, southeastern Mexico, are inferred from a mangrove sediment core deposited between the middle and late Holocene (~5600–1700 cal yr B.P.) in the Rio Hondo Delta. Fossil pollen and concentrations of Ca and Fe and Ca/Fe ratio in sediments are used to record changes in vegetation and climate. Palaeoecological and palaeoclimatic interpretations obtained from pollen abundances and associations and Fe/Ca ratio coincide with dynamics of major global forcings of climate change like ITCZ, ENSO and global cooling. Mesic conditions enabled tropical forest expansion during the middle Holocene (~5600–3650 cal yr B.P.), although there were periodic dry episodes at ~5200 cal yr B.P. and at ~4300 cal yr B.P. that caused disturbance and enabled herbaceous vegetation to expand. Changes in sedimentation and a gradual change from semi-evergreen to dry tropical forest occurred at ~3650 cal yr B.P., with increasing ENSO activity and southward migration of the ITCZ during transition of the middle to late Holocene. The driest period and lowest forest cover occurred between ~2600 and 2000 cal yr B.P. Data show that over the last two millennia, influence of the ENSO on southeastern Mexico is stronger compared to other proxy-records of climate variability from the Caribbean region.

1. Introduction

Holocene climate has been studied from different scientific perspectives, however, the response of ecosystems to hydroclimate variability is still not well understood (Metcalfe et al., 2015; Roy et al., 2017a). A number of palaeoclimate records from around the globe display patterns of climate dynamics that can be explained by orbitally driven summer insolation (Gray et al., 2010; Hodell et al., 2001). The El Niño Southern Oscillation (ENSO) was also established during the Holocene (Rollins et al., 1986; Sandweiss et al., 1996). Other climate forcing mechanisms include migration of the Intertropical Convergence Zone (ITCZ, Haug et al., 2001; Wanner et al., 2008) and changes in North Atlantic Oscillation (NAO, Jury et al., 2007). Climate instability of the early to middle Holocene was related with glacier dynamics in the Northern Hemisphere (Baker et al., 2017). Forest cover was reduced during the middle to late Holocene in several tropical and subtropical areas (Islebe et al., 1996; Mueller et al., 2009; Russell et al., 2003) and is related to a change in precipitation between 6000 and 5000 cal yr B.P. (Magny and Haas, 2004; Mayewski et al., 2004; Wanner et al., 2008). This vegetation change can be related to a global cooling around 5.2 kyr B.P. described by Thompson et al. (2002, 2006). Although their research was based on a Kilimanjaro ice core from east Africa, the authors suggest that the detected climate changes were part of a global climate adjustment. Pollock et al. (2016) attributed precipitation changes in Northern Central America and the Yucatán Peninsula during this period to changes in the North Atlantic Oscillation. Nevertheless, their results do not support NAO as the main climate driver in the Caribbean. They concluded that the northward position of the ITCZ and intensified monsoon in the region could have “damped” NAO and other Atlantic Ocean dynamics. It has been suggested that this event formed part of the middle to late Holocene transition, and an abrupt change in global climate around 4000 cal yr B.P. marked the formal end of the middle Holocene and beginning of the late Holocene (Walker et al., 2012).

All these mechanisms were responsible of changes in both temperature and humidity at different temporal scales that ultimately affected vegetation types. Additionally, sea level changes induced environmental change and established the conditions of the late Holocene

* Corresponding author.
E-mail address: gislebe@ecosur.mx (G.A. Islebe).

https://doi.org/10.1016/j.palaeo.2018.01.014
Received 13 September 2017; Received in revised form 10 January 2018; Accepted 11 January 2018
Available online 31 January 2018
0031-0182/

(Khan et al., 2017). There is also evidence of abrupt changes caused by major climate forcings like solar variability (Mayewski et al., 2004; Wanner et al., 2008). The Yucatán Peninsula in southeastern Mexico presents a complex palaeoecological and palaeoclimatological history because of its geographic position in relation to past and present climatic processes (Orellana et al., 2003; Roy et al., 2017a). Haug et al. (2003) provided evidence of the teleconnection between the Cariaco Basin hydrological system with Yucatan peninsula precipitation change during the Holocene and Hodell et al. (2007) found changes in precipitation in the central Yucatan peninsula were similar to hydrology of the Cariaco Basin. Although the Caribbean records show the ITCZ as a major forcing of climate change in the region, Haug et al. (2001) suggested that the highly variable period between ~3500 and ~2600 cal yr BP was related with the onset of increasing ENSO activity. Nevertheless, all the previous authors recognized that chronology of sedimentary sequences can be improved. The ancient Maya culture also influenced landscape and forest ecosystems since the late Holocene (Anselmetti et al., 2007; Gill, 2001; Islebe et al., 2015b; Lentz et al., 2014). Human activities are present since the middle Holocene (Pohl et al., 1996) and evidences suggest forest management strategies and a close relationship between the forest and inhabitants of the Maya region (Ford, 2008; Ford and Nigh, 2009). Although there is evidence of forest clearance in the Maya lowlands in northern Petén (Rosenmeier et al., 2002), the Yucatan peninsula records do not show major forest reductions during the Maya occupation (Aragón-Moreno et al., 2012; Carrillo-Bastos et al., 2010; Torrescano-Valle and Islebe, 2006, 2015).

The palaeo-records have shown that the middle Holocene was a period of increased precipitation in the Caribbean area (Carrillo-Bastos et al., 2010; Torrescano-Valle and Islebe, 2015), whereas the transition to the late Holocene was marked by distinctive periods of reduced precipitation (Carrillo-Bastos et al., 2013; Haug et al., 2001; Hodell et al., 2007). So far, few palaeoecological records from the Peninsula extend to the middle Holocene, with most of the records covering the late Holocene. Carrillo-Bastos et al. (2010) presented pollen and isotope data from the Lake Tzib, on the central Yucatan Peninsula, and reported a steady decrease in precipitation between 6000 and 4700 cal yr B.P. Torrescano-Valle and Islebe (2015) studied pollen data from a sediment core taken in the Lake Silvituc in south-central part of the peninsula and reported changes in vegetation composition associated with humid and dry intervals. These changes were attributed to ITCZ displacement that played a major role in the regional precipitation pattern. The ITCZ shifts to a northern position during the wet season and to the south during the dry season. This latitudinal movement was the basis for an integrative model of precipitation change in the Caribbean region during the late Holocene (Haug et al., 2001).

Another major climate driver for the region is ENSO variability, which is related to sea surface temperature (SST) anomalies at different temporal and spatial scales. In the Caribbean region, ENSO activity is related to changes in precipitation, vegetation and cyclone formation (Klotzbach, 2011). In this regard, Jennerjahn et al. (2004) highlighted the importance of regional climate and hydrology determining modern and future ecological responses to specific forcings. It is evident that ITCZ dynamics are connected to ENSO activity (Muñoz et al., 2017). Hence, an understanding of this interaction is crucial to comprehend ecosystem response to changing conditions. Our main objective was to determine vegetation response to major climate forcings in the southeastern part of the Yucatan Peninsula, Mexico during the middle and late Holocene, and to understand the observed environmental changes in the framework of the broader Caribbean region.

2. Study site

The Río Hondo is a fluvial basin that politically divides Mexico from Belize and is a major water system on the eastern Yucatán Peninsula that discharges into Chetumal Bay, in the Caribbean Sea (Fig. 1). It is a semi-closed system connected with the Mesoamerican Reef in the Caribbean Basin. This basin receives annual precipitation of 1300 mm, distributed mainly during the rainy season from May to November, and the mean annual temperature is 26.5 °C (Orellana et al., 2003). Rainfall is determined by annual changes in the ITCZ position, which depends of the atmosphere-ocean interaction in the tropical Atlantic. Easterly trade winds, intensified by an increased North Atlantic Subtropical High (NASH), increases transport of humidity from tropical Atlantic to the Caribbean Basin. Humidity continues to move across the Caribbean by the Caribbean Low Level Jet (CLLJ), which moves the ITCZ northward during boreal summer and brings precipitation to the entire Caribbean region, including central America and Yucatan Peninsula (Muñoz et al., 2008). The ITCZ migrates southward during the boreal winter and precipitation decreases in the entire Caribbean region.

The coring site was located in the delta of the Río Hondo (18°29′20.00″N, 88°19′10.00″W, Fig. 1). Riverine mangroves grow along the shore, with *Rhizophora mangle* as the dominant species, representing almost 80% of the mangrove cover. *Thrinax radiata* and *Pachira aquatica* are also well represented in the area (Tovilla-Hernández et al., 2009). Surrounding vegetation is composed by semi-evergreen tropical forest (Sánchez-Sánchez and Islebe, 2002), characterized by species of the *Moraceae*, *Sapotaceae*, Meliaceae, Fabaceae, Burseraceae, Anacardiaceae and Bignoniaceae families, among others (Torrescano-Valle and Islebe, 2006).

3. Materials and methods

A sediment core was retrieved in 50-cm-long sections to a maximum depth of 8 m, using a Russian corer. Sampled sections were photographed in the field, packed to avoid contamination and humidity loss and transported to the Palynology Laboratory of the El Colegio de la Frontera Sur for subsequent processing. Bulk sediment organic matter at depths of 797, 478 and 190 cm were dated by the Accelerator Mass Spectrometry (AMS) radiocarbon technique at Beta Analytic to establish a chronology for the sediment column (Table 1). The use of bulk organic material for radiocarbon dating was applied because sediments from Río Hondo are composed mainly by runoff bearing sediments and there were no apparent leaf fragments or other macrobotanical remains to date. Radiocarbon dates were calibrated using IntCal13 curve in Calib 7.10 software (Reimer et al., 2013; Stuiver et al., 2017) into calendar years (1 cal yr B.P. = 1950 CE). Additional time control was achieved by comparing our geochemical data with the Ti data of Cariaco (Haug et al., 2001).

The upper 105 cm of the sediment core showed poor pollen preservation. A total of 133 sub-samples, collected at different intervals between depths of 800 and 105 cm, were processed with hydrochloric acid, potassium hydroxide, sodium pyrophosphate (Bates et al., 1978) and suspended in zinc bromide (Nakagawa et al., 1998) for pollen isolation. A *Lycopodium* spore tablet was added for laboratory control. Acetolysis was applied to enable detailed pollen structure identification (Faegri and Iversen, 1989). At least 300 pollen grains, mounted on slides, were counted as a pollen sum, and identified with an optical microscope (400×). Pollen taxa were pooled into ecological groups based on vegetation surveys and ecological affinities of taxa. Identification of rare pollen types was achieved consulting the ECOSUR herbarium pollen reference collection and Palacios-Chávez et al. (1991). A total of 297 sub-samples, taken every 2–3 cm between 800 and 105 cm depth, were prepared for X-ray fluorescence (XRF) analysis and included all sample depths selected for pollen analysis. Samples were oven-dried for 24 h at 60 °C, homogenized and labelled individually. Concentrations of calcium (Ca) and iron (Fe) were measured using a Thermo Scientific Niton XL3t X-ray fluorescence (XRF) analyzer and values were subsequently corrected as suggested by Roy et al. (2017b).

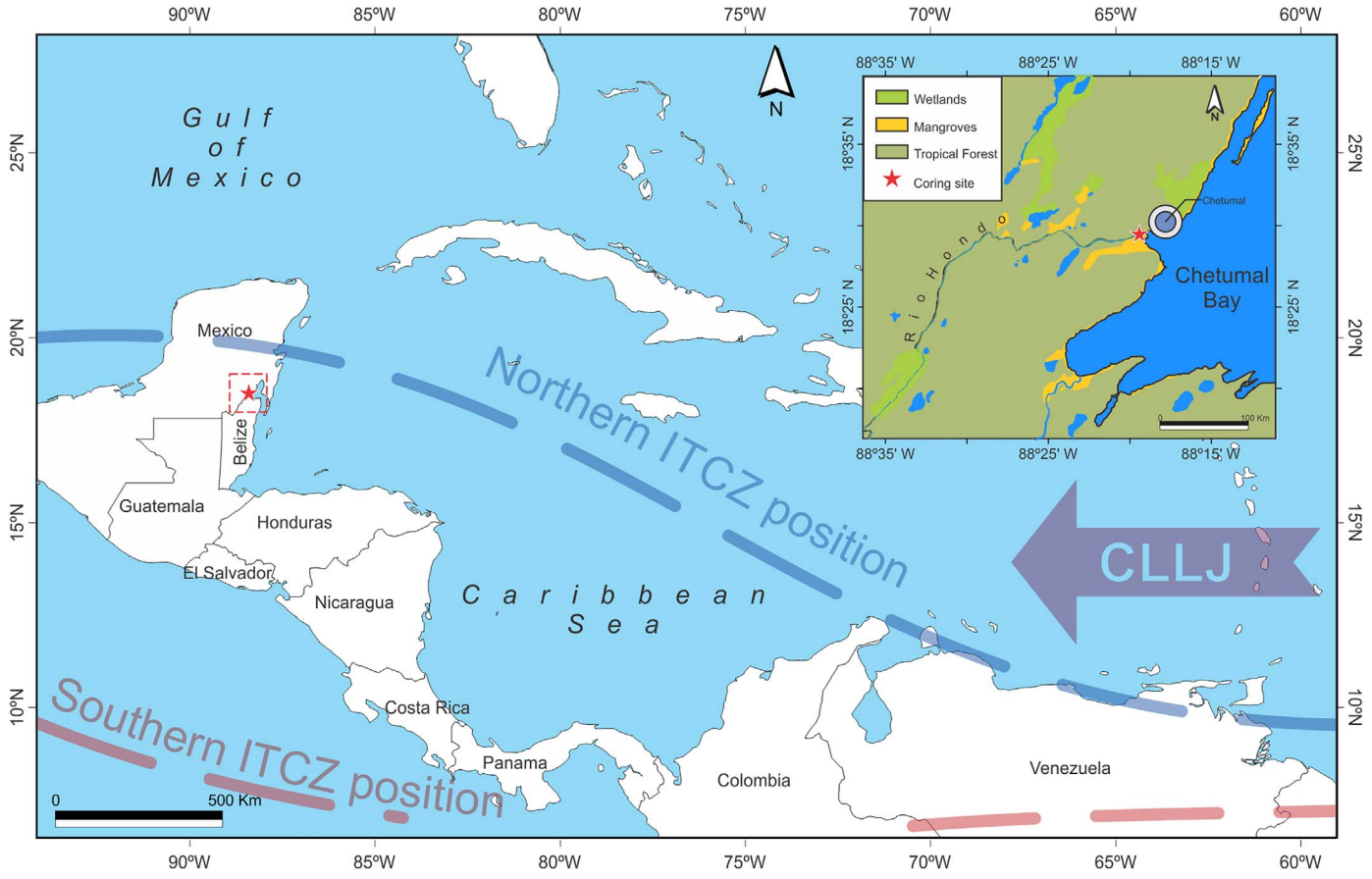

Fig. 1. Location map of the Río Hondo in southeastern Yucatan Peninsula of Mexico. Dashed lines represent the modern Intertropical Convergence Zone (ITCZ) position during wet (blue) and dry (red) seasons. Formation of the Caribbean Low Level Jet (CLLJ) transports humidity into the region from the eastern Caribbean Sea. Map was drawn based on information from Haug et al. (2003) and Muñoz et al. (2008). (For interpretation of the references to color in this figure legend, the reader is referred to the web version of this article.)

4. Results

4.1. Core description

The sediment core was composed of peat, fine and medium sand, silty-clay and clay. Yellowish (800–797 cm) and medium gray clay (797–794 cm) were found at the base of the core. Silty-clay constitutes the sediment between depths of 794 and 140 cm and there are differences in color along the length of the sediment column. Sporadic bands of gray occur at depths of 494, 463, 440, 434 and 348–345 cm, and sediments of 376–356 cm have yellowish tone. Medium and fine sand are present at depths of 140–97 cm and sediments from 95 to 84 cm constitute silty-sand. Consolidated peat layers are present at depths of 97–95 and 84–70 cm, and the upper part of the core (70–0 cm) was composed of unconsolidated peat, mixed with sand of different grain sizes.

4.2. Chronology

The age vs. depth relationship in the core was established by linear interpolation between adjacent calibrated radiocarbon ages and extrapolation beyond the youngest date (Fig. 2). Bulk organic matter at 797 cm depth has a median probability age of 5590 cal yr B.P. The AMS dates obtained from bulk organic matter at depths of 478 cm and 190 cm yielded ages of 5156 cal yr B.P. and 2464 cal yr B.P., respectively (Table 1). Four additional samples were dated of gasteropod shells, but were discarded for the age-depth model, because of the reservoir effect (Table 1). Although Kovacs et al. (2017) found a hard water error of ~1300 yrs. similar to Curtis et al. (1996), the uncertainty calculation may have varied between samples and the inclusion of dates into the age model do not apport additional information of changes in sedimentation. The sedimentation rate was higher between 5590 and 5160 cal yr B.P. (0.39 cm/yr) compared to the sediments deposited between 5160 and 1690 cal yr B.P. (0.11 cm/yr), representing 478–105 cm depth of the core.

Table 1
Radiocarbon ages and calibrated dates of sediments collected from the Río Hondo Delta, southeastern Yucatan Peninsula, Mexico.

Lab code	Depth (cm)	Material	Radiocarbon age	2σ probability	Median probability age (cal yr B.P.)
Beta - 377,104	190	Bulk organic	2460 ± 30 BP	0.711	2464
Beta - 446,133	478	Bulk organic	4530 ± 30 BP	0.652	5156
Beta - 438,439	797	Bulk organic	4860 ± 30 BP	0.315	5590
Beta - 373,842	366	Shell	5060 ± 30 BP	1.0	5827
Beta - 377,105	470	Shell	5570 ± 30 BP	1.0	6361
Beta - 377,106	616	Shell	5340 ± 30 BP	1.0	6154
Beta - 373,843	761	Shell	5420 ± 40 BP	1.0	6234

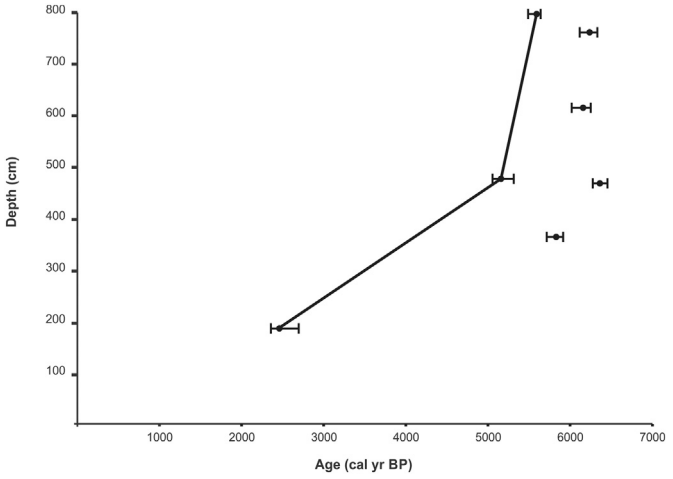

Fig. 2. Age model for the sediment sequence reconstructed using calibrated radiocarbon age vs. depth of three samples from the core. Radiocarbon dates from *Pyrgophorus sp.* shells were plotted, but excluded from the age model due to uncertainty in the calculation of reservoir effect.

4.3. Pollen and XRF analysis

The pollen diagram was plotted with 68 identified taxa distributed in 39 families from sediments deposited between 800 and 105 cm depth (Fig. 3). Sub-sampling provides a temporal resolution of ca. 6 yrs in the lower part of the core (797–478 cm, 5590–5160 cal yr B.P.) and ca. 60 years in the upper section (478–106 cm, 5160–1700 cal yr B.P.). Five major pollen zones were identified (Fig. 4) using Constrained Incremental Sum of Squares (CONISS) cluster analysis, included in Tilia software (Grimm, 2016).

Concentration of titanium (Ti) is below the detection limit of the XRF analyzer except for the 46 samples between depths of 230 and 149 cm (2840–2080 cal yr B.P.). These sediments contain 0.10–0.24% Ti. Both calcium (Ca) and iron (Fe) were measured in sediments throughout the entire core. Sediments have variable concentrations of Ca (11.1–37.3%, average = 30.9%) and Fe (0.2–1.3%, average = 0.3%) (Fig. 4). Ca and Fe show inverse distributions ($r = -0.9$, $p < .05$), which suggests the association of Ca with carbonate minerals and Fe with non-carbonate minerals (oxides and clay). Higher values of Ca compared to Fe reflects the influence of the karst nature of the Yucatán Peninsula on the chemical composition of sediments deposited in the Río Hondo Delta. We used the Ca/Fe ratio to estimate the abundance of Ca-bearing carbonates with respect to the abundance of Fe-bearing oxides/clay minerals in sediments deposited between 5600 and 1690 cal yr B.P. and report the geochemical characteristics of sediments in the five identified pollen zones in Fig. 4. These geochemical proxies were compared with their average values throughout the core to illustrate the relative abundances of carbonate and non-carbonate minerals in the sediment core. Sediments of zones I, II and III have comparable and homogenous geochemical characteristics compared to the heterogeneous sediments of zone V. Concentrations of Ca and Fe and the Ca/Fe ratio show intermediate variations in sediments of the zone IV.

4.3.1. Zone I (800–503 cm, 5600–5200 cal yr B.P.)

Mangrove is represented by pollen of four species, i.e. *Rhizophora*

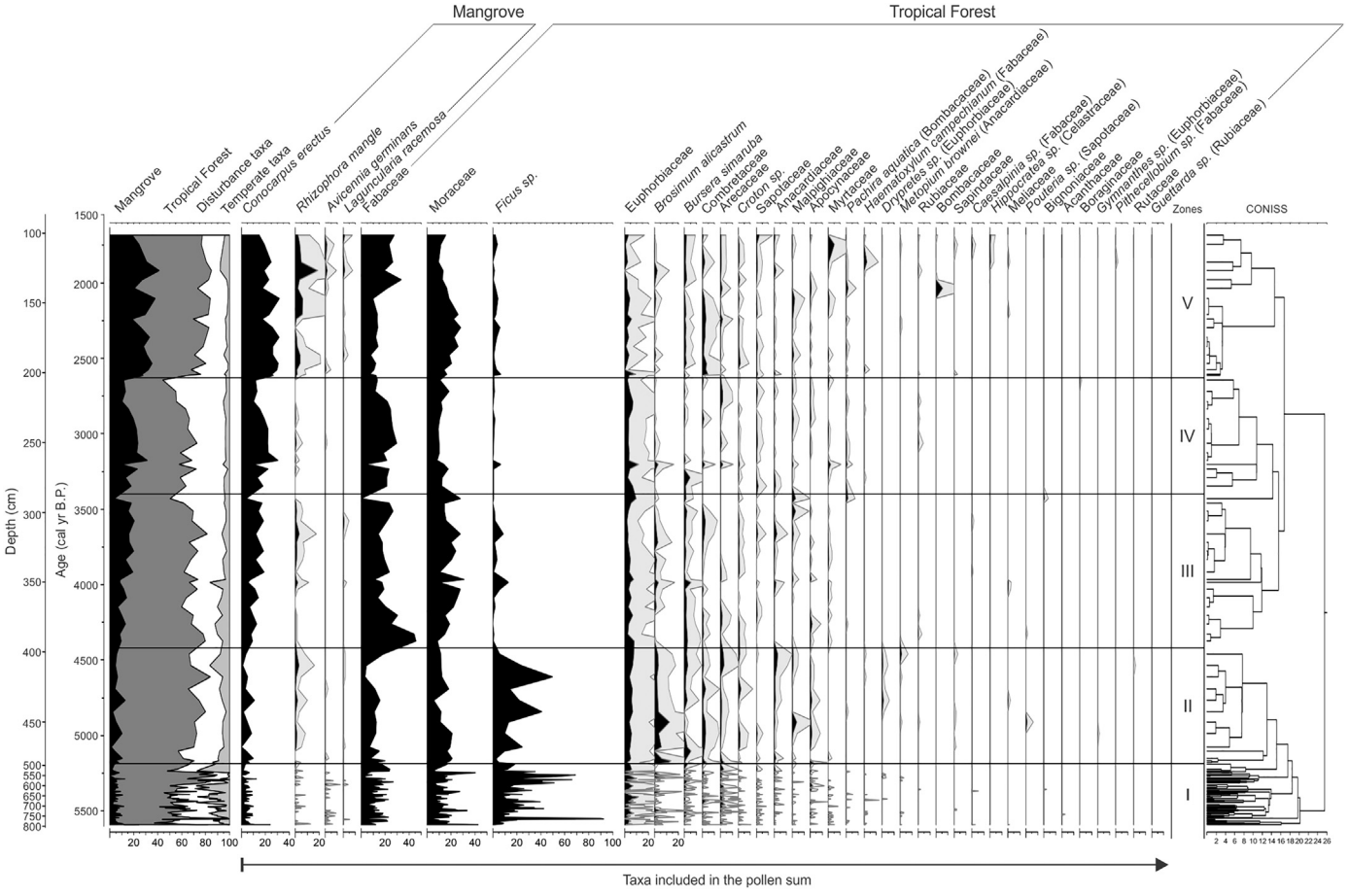

Fig. 3. Pollen diagram representing percentages of total pollen from mangrove, tropical forest, disturbance taxa, temperate taxa and aquatic vegetation in sediments collected from the Rio Hondo, southeastern Yucatan Peninsula, Mexico. The pollen taxa are grouped by ecological affinities and pollen zones was determined by CONISS (Grimm, 1987).

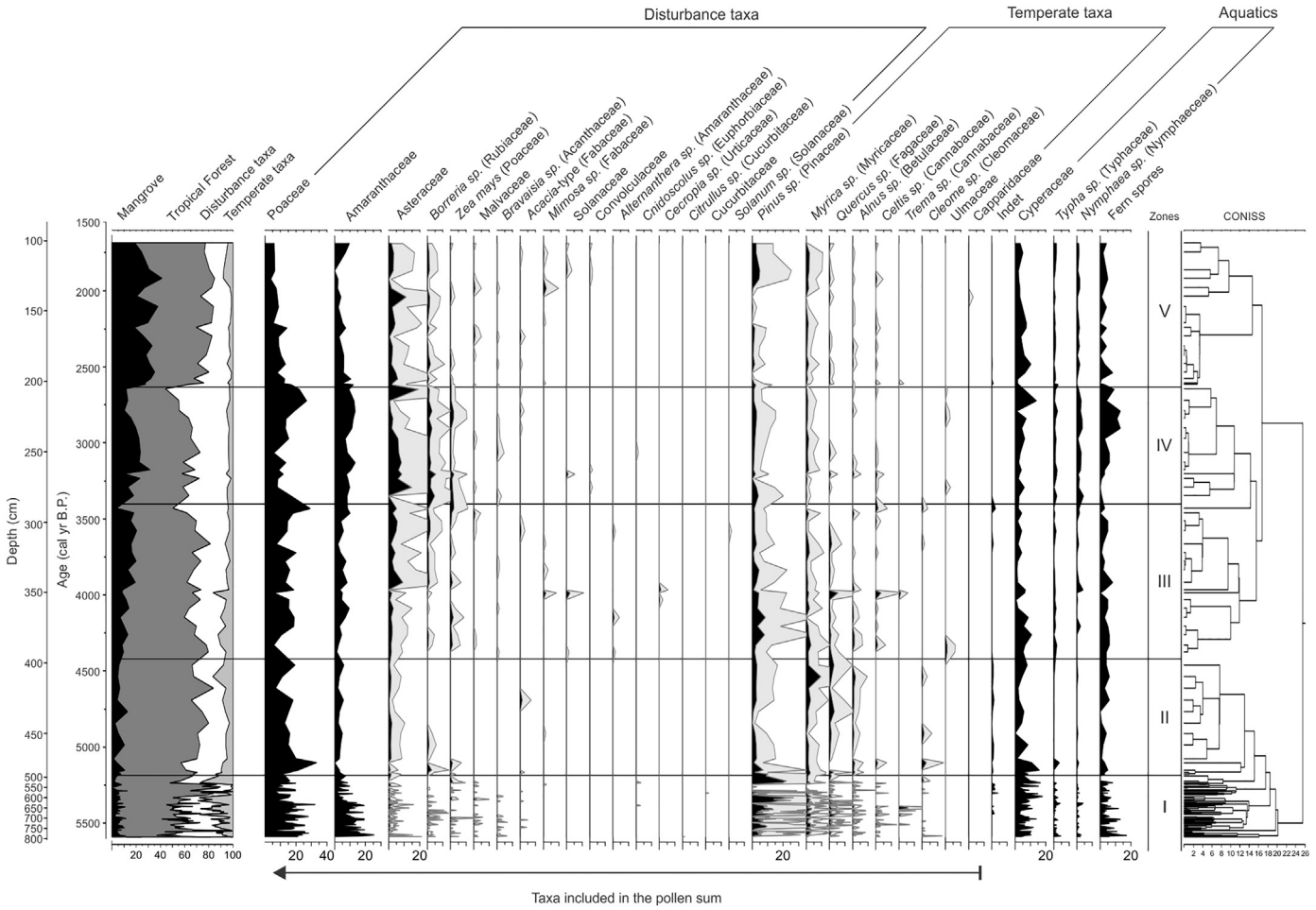

Fig. 3. (*continued*)

mangle, *Conocarpus erectus*, *Laguncularia racemosa* and *Avicennia germinans*. *Conocarpus erectus* is the best represented taxon with values > 10% and has abundances of 24% and 12% in sediments deposited at 5600 cal yr B.P. and 5300 cal yr B.P., respectively. *Rhizophora mangle* has its highest value (2.6%) at 5600 cal yr B.P. Pollen of *Ficus sp*. is the most abundant among the tropical forest taxa and represents 1.1–93% of the pollen sum. Other Moraceae represent the second most abundant taxa, with abundances of 1.8–43%. Fabaceae is present throughout almost the entire zone and *Brosimum alicastrum* is not present continuously. Euphorbiaceae, *Bursera simaruba* and Arecaceae appear sporadically, whereas other taxa like *Pachira aquatica*, Sapotaceae, *Haematoxylum campechianum*, Malpighiaceae and *Metopium brownei* are rare, with values < 1%. Poaceae and Amaranthaceae are the most abundant pollen types of disturbance vegetation, and Asteraceae and *Borreria sp*. (Rubiaceae) are often present. *Zea mays* appears sporadically and is recorded since the beginning of this pollen zone. Its highest value (3.3%) is observed at 5500 cal yr B.P. Temperate taxa are represented by *Pinus sp*. (0–27%) and *Myrica sp*. (0–6%) is the second most important taxon. *Quercus sp*., *Alnus sp*., *Celtis sp*. and *Trema sp*. are recorded regularly, with abundances < 6%.

Sediments of this zone have relatively higher Ca (28.8–35.2%) and lower Fe (0.2–0.3%). In general, Ca concentration is above the average value of sediments of the entire core and concentrations of Fe remain below average (Fig. 4). The Ca/Fe ratio (92–209) estimates the abundance of Ca-bearing carbonate minerals in comparison with the Fe-bearing oxides and clays. It is above average in the zone, except for sediments deposited at 5600 cal yr B.P. and 5400 cal yr B.P. Sediments deposited at those times are characterized by below average Ca/Fe, which indicates relatively less deposition of Ca-bearing carbonates or greater deposition of Fe-bearing oxides and clays in comparison with other sediments in this interval.

4.3.2. Zone II (503–399 cm, 5200–4400 cal yr B.P.)

Mangrove is represented by 0–11% of *Conocarpus erectus* and almost continuous presence of *Rhizophora mangle* (< 3.1%). *Avicennia germinans* and *Laguncularia racemosa* appear sporadically, with relatively higher abundances compared to the previous zone. Pollen diversity of tropical forest taxa increases. *Ficus sp*. percentages fluctuate abruptly, whereas Fabaceae, Moraceae and Euphorbiaceae remain relatively constant. *Brosimum alicastrum* appears in the entire zone with abundances between 2 and 14%. *Bursera simaruba*, Combretaceae, Arecaceae, *Croton sp*., Anacardiaceae, Malpighiaceae and Apocynaceae appear continuously with low values. *Pachira aquatica* appears at 4800 cal yr B.P., with abundance of < 1%. *Metopium brownei* appears sporadically at the end of this pollen zone. *Hippocratea sp*., *Pouteria sp*., *Gymnanthes sp*. and Rutaceae appear rarely. Abundances of disturbance taxa decrease compared to the previous zone, Poaceae is again the most representative taxon of disturbance vegetation (7–22%). Asteraceae decrease and the abundance of *Borreria sp*. remains constant from 5200 to 4900 cal yr B.P. *Zea mays* appears only at 5200 and 5100 cal yr B.P. Taxa with temperate affinity decline. *Pinus sp*. is present with values < 4%. Its abundance increases to 10.3% and 7.1% at ca. 5200 cal yr B.P. and 5150 cal yr B.P., respectively. *Myrica sp*. remains constant during this zone (< 3%) and increases to 9% at 4500 cal yr B.P. *Quercus sp*. and *Alnus sp*. appear sporadically. *Celtis sp*. and *Trema sp*. are present, but in lower percentages.

Concentrations of Ca (28.0–35.9%) and Fe (0.2–0.4%) in sediments of this zone are comparable to sediments of zone I. Ca values, in

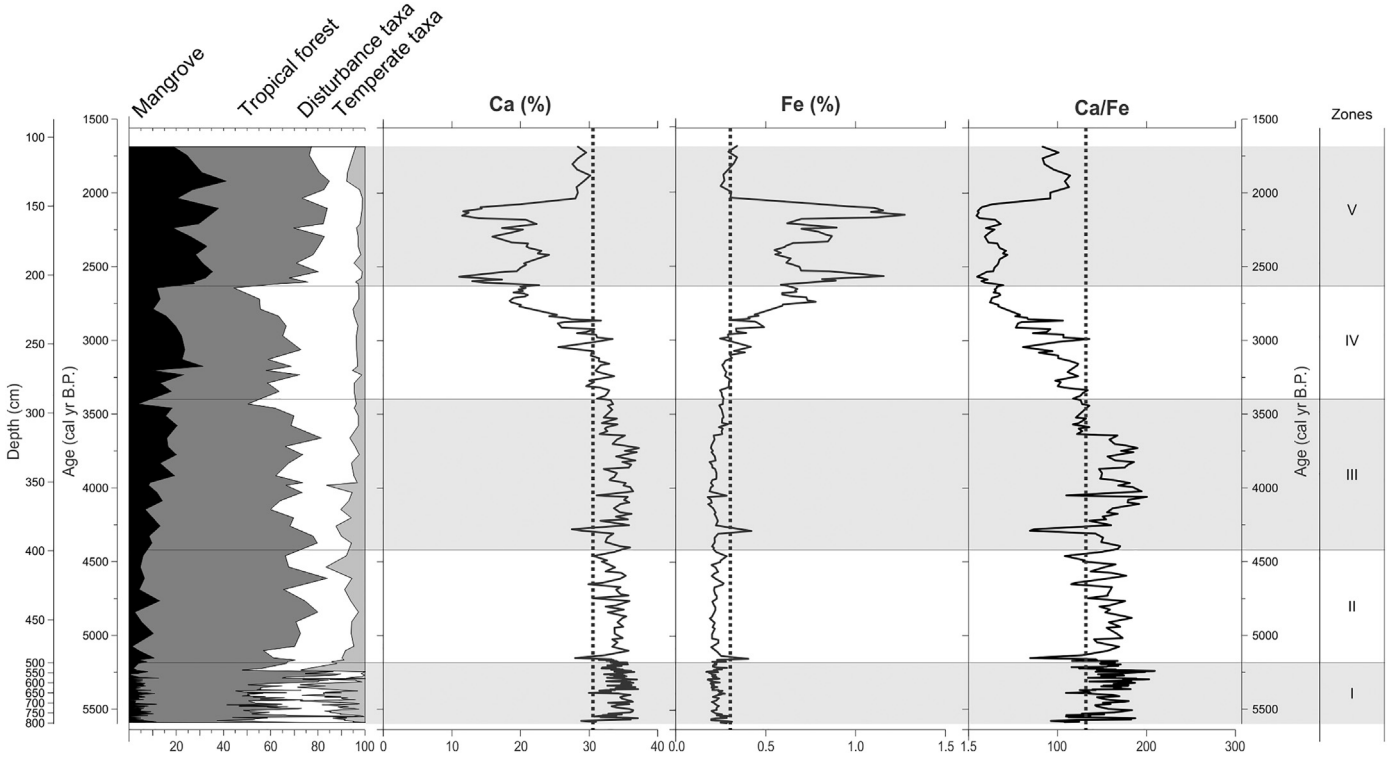

Fig. 4. Summary diagram of total pollen percentages and geochemical characteristics of the Rio Hondo core, characterized by Ca and Fe concentrations and the Ca/Fe ratio. Dotted lines indicate their average values and the shaded areas correspond to the pollen zones.

general, are above average and Fe concentrations remain below average. Sediments of this zone have above average values of Ca/Fe (69–183), except at ca. 5150, 4650 and 4460 cal yr B.P. Sediments deposited at those times have relatively less Ca-bearing carbonates or higher Fe-bearing oxides and clays compared to rest of the sediments of this zone.

4.3.3. Zone III (399–290 cm, 4400–3400 cal yr B.P.)

Mangrove vegetation displays an increasing trend, especially *Conocarpus erectus*. *Rhizophora mangle* appears regularly between 4000 and 3500 cal yr B.P. Tropical forest taxa decrease, while the overall number of taxa increases. Fabaceae is the best represented tropical forest taxon, reaching values > 40% from 4400 to 4300 cal yr B.P., but displays a general decreasing trend until the upper part of the pollen zone, disappearing at 3400 cal yr B.P. *Bursera simaruba* maintains low values, < 3%, except at 4000 cal yr B.P. when it has a peak of almost 6%. Moraceae values oscillate between 10 and 30% in this pollen zone, despite abrupt percentage changes between 4000 and 3900 cal yr B.P., when their abundance reach the lowest and highest values in this time interval. *Ficus sp*. almost disappears, however it peaks at 4000 and 3700 cal yr B.P. *Brosimum alicastrum* appears in lower percentages than the previous period while other tropical forest taxa appear occasionally. Disturbance vegetation increases, Poaceae varies considerably along the section. Asteraceae remains relatively constant at the beginning of this zone, until around 3900 cal yr B.P. when it peaks. *Borreria sp*. appears regularly during this period, although with values are < 2%. *Zea mays* is regularly found with values < 1%, except at 3900 and 3400 cal yr B.P. when they peak 1.3 and 2.2%, respectively. Other disturbance taxa appear sporadically and temperate taxa decrease continuously, although diversity remains similar to the values in the previous zone.

Sediments of this zone also have concentrations of Ca (27.5–37.3%) and Fe (0.2–0.4%) comparable to sediments of zones I and II. The Ca/Fe ratio, however, is more variable (67–200) compared to the two previous zones. Sediments deposited during 3650–3400 cal yr B.P. have average values of Ca/Fe and sediments deposited at 4300 cal yr B.P. and 4100 cal yr B.P. have below average Ca/Fe.

4.3.4. Zone IV (290–208 cm, 3400–2600 cal yr B.P.)

Mangrove vegetation is almost exclusively represented by *Conocarpus erectus*, and *Rhizophora mangle* appears rarely. Tropical forest cover continues to decrease, although diversity of pollen taxa remains constant. Fabaceae is the most important tropical forest taxon, with fluctuating values > 20% between 3400 and 2800 cal yr B.P., except at 3200 cal yr B.P. when they almost disappear. Moraceae fluctuate around 15%, while *Ficus sp*. values remain < 2%. Euphorbiaceae occurs continuously with low values, except at 3200 cal yr B.P. when it peaks at about 12%. Disturbance vegetation increases, although Poaceae percentages decrease compared to the previous zone. Amaranthaceae has percentages between 7 and 13%. Asteraceae broadly fluctuates from 0 to 15% between 3300 and 3200 cal yr B.P. This is followed by a decreasing trend, but its highest value (19%) at 2600 cal yr B.P. *Borreria sp*. appears continuously. *Zea mays* occurs in this pollen zone with values around 2%. Other disturbance taxa appear occasionally, with values < 2%. Temperate taxa decrease, although *Pinus sp*. persists continuously. *Myrica sp*. is found almost continuously, except at 3200 cal yr B.P. when it disappears.

Sediments of this zone display variable geochemical characteristics. Concentrations of Ca (18.4–33.7%) can be found both above average and below average for the whole core. Similarly, some of the sediments have below average and other have above average Fe (0.3–0.8%). The abundance of Ca-bearing carbonate minerals is lower than that in sediments of the previous zones (I, II and III). Similarly, the abundance of Fe-bearing oxides and clays is higher in this zone compared to the previous zones. Ca/Fe (24–136) varies between average and below-average, and it displays a gradually decreasing trend from the bottom to the top of this zone. It indicates gradually decreasing abundance of Ca-bearing carbonate minerals in comparison with Fe-bearing oxides and clay from 3400 to 2600 cal yr B.P.

4.3.5. Zone V (208–105 cm, 2600–1700 cal yr B.P.)

Mangrove representation increases and *Conocarpus erectus* is still the most abundant mangrove taxa. Although *Rhizophora mangle* appears in the entire zone (1–6%), with a peak of 19% at 1700 cal yr B.P and *Laguncularia racemosa* appears intermittently, with values < 2%. Tropical forest taxa slightly increase their representation. Fabaceae remains relatively constant until 2000 cal yr B.P. Its highest abundance (33%) is present at 2000 cal yr B.P. Moraceae increase steadily up to 26% until 2200 cal yr B.P. and their lowest value (10%) is observed at 1900 cal yr B.P. *Ficus sp*. and Euphorbiaceae appear regularly, but with low abundances. *Brosimum alicastrum* appears regularly. *Bursera simaruba*, Combretaceae, Arecaceae, *Croton sp*. and Sapotaceae appear regularly. *Pachira aquatica* appears continuously between 2500 and 2400 cal yr B.P. and again between 2000 and 1900 cal yr B.P. *Haematoxylum campechianum* occurs between 1920 and 1860 cal yr B.P. Bombacaceae abundance increase to 6% at 2000 cal yr B.P. Sapindaceae, *Caesalpinia sp*., *Hippocratea sp*. and Meliaceae are found from 1900 to 1700 cal yr B.P. Abundances of disturbance taxa decrease. Poaceae and Amaranthaceae follow a decreasing trend, while Asteraceae percentages remain constantly low and *Borreria sp*. appears regularly with low values. *Zea mays* appears discontinuously, with values of < 1%. *Pinus sp*. is the most abundant pollen type of temperate vegetation.

Geochemical characteristics of sediments of this zone show the greatest variability. Concentrations of Ca (11.1–30.2%) are below average and Fe values (0.3–1.3%) are average to above-average. Ca/Fe (9–114) remains below average. There is a minor increase in the abundance of Ca-bearing carbonates between 2000 and 1700 cal yr B.P.

5. Discussion

5.1. Palaeoecological reconstruction

Fossil pollen preserved in sediments deposited in the Rio Hondo Delta record local and regional vegetation changes of coastal and continental environments on the southeastern Yucatan Peninsula between 5600 and 1700 cal yr B.P. The Ca/Fe ratio reveals deposition of Ca-bearing carbonate minerals in comparison with Fe-bearing oxides and clays, and reflects the fluvial dynamics of the basin, associated with precipitation and riverine discharge (Fig. 4). Due the karstic geology of the Yucatan peninsula, the intervals of increase in precipitation and more fluvial discharge of the Rio Hondo would transport Ca-rich sediments in comparison with Fe-rich sediments from the drainage basin. We have reconstructed changes in runoff associated with the intervals of variable precipitation by using the Ca/Fe ratio. It, however, differs with other records from the siliciclastic watershed where Fe-rich sediments increase in comparison with Ca-rich sediments during the humid periods. There was greater erosion and dissolution of the limestone of the Yucatan Peninsula during the humid intervals, i.e. with more precipitation and stronger fluvial discharge (Beach et al., 2008), which led to more Ca-bearing carbonate minerals deposited in the Rio Hondo Delta. Conversely, during the arid periods, deposition of Fe-bearing oxides and clays increased in comparison with Ca-bearing carbonates (Fig. 4) and we corroborated this by documenting increased tropical forest taxa during the episodes of enhanced Ca-bearing sediment deposition (Fig. 4). In general, sediments with above-average values of Ca/Fe were deposited between 5600 and 3650 cal yr B.P. and these sediments preserve fossil pollen taxa indicating a humid environment represented by tropical forest, temperate vegetation, savannas, wetlands and semi-evergreen forests. We present the reconstructed palaeovegetation and palaeoclimate for two intervals, using the pollen and geochemical data, i.e. 5600–3650 cal yr B.P. and 3650–1700 cal yr B.P. (Fig. 5).

5.1.1. 5600–3650 cal yr B.P

Above-average values of Ca/Fe suggest that the area received higher precipitation and stronger fluvial activity during this interval. This time period is represented by the development of extensive tropical forest, temperate vegetation, savannas and wetlands. Pollen composition suggests mesic conditions and high diversity of environments (Torrescano-Valle and Folan, 2015), conditions that are in agreement with regional settings described by Islebe et al. (1996) in the Maya lowlands during the middle Holocene, when high forest dominated the landscape. Poaceae is the best represented disturbance taxa with Amaranthaceae, although their presence is more associated with natural savannas, wetlands and coastal vegetation (Islebe et al., 2015a; Torrescano-Valle and Folan, 2015) in northern Belize (Bridgewater et al., 2002). Disturbance taxa associated with human activities or drought-tolerant taxa like Asteraceae and Malvaceae were less important. Nevertheless, *Zea mays* pollen appears regularly, beginning at the base of the core (i.e. 5600 cal yr B.P.).

Although climatic conditions enabled the development of extensive tropical forest, there were highly variable periods when Moraceae, Fabaceae and *Ficus sp*. fluctuated according to changes in precipitation. The increase in *Borreria sp*. and *Bravaisia sp*. could be associated with periods of reduced precipitation (drought) and/or increased soil salinity caused by reduced freshwater input (Chauhan and Johnson, 2008; Moreno-Casasola and Espejel, 1986), though overall these taxa occur during isolated intervals at low percentages. Presence of tropical forest taxa like Sapotaceae, *Haematoxylon campechianum*, *Pouteria sp*., *Pachira aquatica*, among others, suggest humid conditions and presence of diverse tropical forest types, wetlands and grasslands. This vegetation composition falls within a period of a northern position of the ITCZ (deMenocal et al., 2000; Giry et al., 2012, 2013; Haug et al., 2001), coupled with cooler Caribbean SST (Giry et al., 2012) and an intensified Caribbean Low Level Jet (Pollock et al., 2016) that favored the development of vegetation types related to humid environments.

These centennial-scale fluctuations in precipitation and fluvial activity are also reflected by below-average values of Ca/Fe, especially at ~5200 cal yr B.P. and around 4300 cal yr B.P. Some of the other events of below average fluvial activities occurred at ~5600, ~5400, ~4700, ~4500 and ~4100 cal yr B.P. Reduced precipitation caused an increase in *Pinus sp*., disappearance of *Brosimum alicastrum* and a reduction in Moraceae at around 5200 cal yr B.P. (5.2 kyr B.P. event). Nevertheless, Fabaceae and Euphorbiaceae increased, Poaceae increased and Amaranthaceae maintained stable with low values, while Asteraceae and Malvaceae were almost absent during this dry period. Other taxa associated with dry forest, such as *Bursera simaruba*, *Croton sp*., Combretaceae, Sapotaceae, Anacardiaceae and Apocynaceae (Islebe et al., 2015a) appeared. However, the interpretations may contain chronological uncertainties at different timescales due to limited radiocarbon analysis.

The southward migration of ITCZ during the middle to late Holocene transition (Haug et al., 2001, 2003) favored disturbance taxa like Poaceae, Asteraceae, *Borreria sp*. among others in some periods at Rio Hondo, although tropical forest remained constant, with slight increases between 5100 and 4300 cal yr B.P. Mangrove vegetation increased despite the drying trend, which was not unexpected, as sea level rose during middle Holocene, when sea level was ~3 m below present, and continued to rise until it stabilized during the late Holocene (Khan et al., 2017; Toscano and Macintyre, 2003).

Dry conditions around 4300 cal yr B.P. were characterized by a reduction in tropical forest, less mangrove (only *Conocarpus erectus*), an abrupt increase in Fabaceae, less Moraceae and disappearance of *Brosimum alicastrum*. Semi-evergreen tropical forest diminished and was replaced by dry tropical forest. Disturbance taxa remained low and Amaranthaceae almost disappeared. Temperate vegetation declined, but *Ulmus sp*. pollen was found. Presence of *Ulmus sp*. suggests that the open vegetation enabled the dispersal of pollen from long distances and altitudes. During the dry episode at around 4000 cal yr B.P., Moraceae abruptly decreased, but Fabaceae remained constant, while Poaceae and Amaranthaceae increased slightly. *Celtis sp*. increased abruptly and

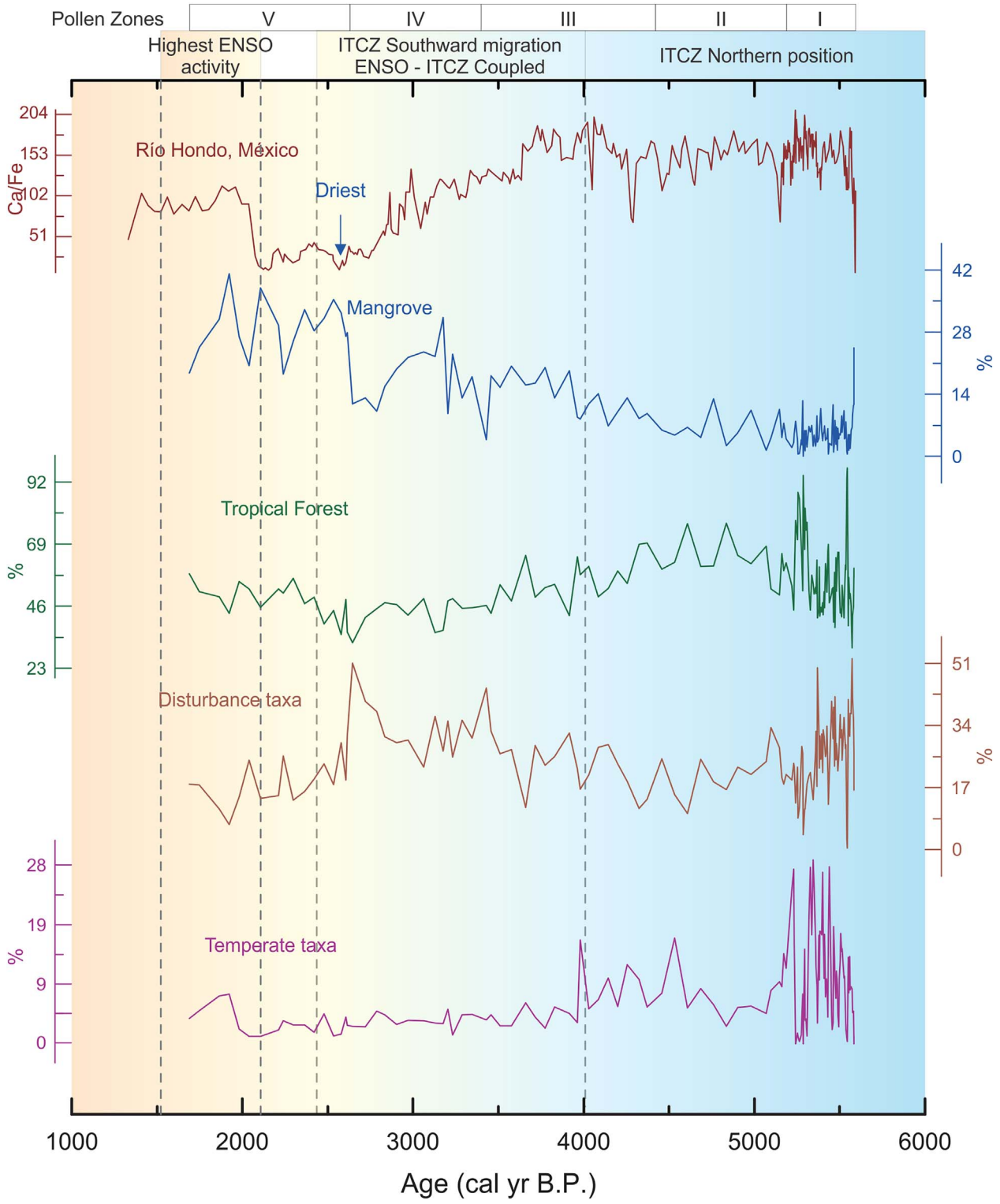

Fig. 5. Summary graph of mangrove, tropical forest, disturbance and temperate pollen taxa compared to Ca/Fe ratio recorded in the Rio Hondo core.

Borreria sp. started to appear constantly. These changes in vegetation composition suggest highly variable environments, which can be related with the onset of the modern ENSO (Fisher et al., 2008) and the formal end of the middle Holocene (Walker et al., 2012). Climate may have varied on annual to decadal timescales and induced successional stages that favored the increase of pioneer species like *Celtis sp*. (Budowski, 1966) and others. Based on study of a core taken 23 km inland from the northwestern Caribbean coast, Torrescano-Valle and Islebe (2006) determined that mangrove vegetation established in the region at around 4600 cal yr B.P. The Rio Hondo Delta core was collected at the river mouth and this configuration may explain the low values of *Rhizophora mangle* throughout the sediment column and the high values of *Conocarpus erectus*, as *R. mangle* occupied only a fringe along the river banks, beyond which there was diverse savanna, wetlands and mixed types of tropical forest, with a transition dominated by *C. erectus*.

Around 3800 cal yr BP, Yao and Liu (2017) reported the progressive replacement of freshwater environments to brackish marsh in part of the Everglades at the same time that mangrove established in the wider Caribbean region. These landscape modifications suggest the higher influence of seawater and sea level stabilization in accordance with sea level curves proposed by Toscano and Macintyre (2003) and Khan et al. (2017). The riverine mangroves of Río Hondo may responded to a coupled effect of decreasing precipitation and the slowing down of sea level rise during this time. *Conocarpus erectus* could be favored by the reduction of precipitation and higher soil salinity and *Rhizophora mangle* do not present significant increase as a result of reduced available habitat caused by coastline definition.

5.1.2. 3650–1690 cal yr B.P

Following the ~4000 cal yr B.P. episode of dry climate, there was progressive southward migration of the ITCZ. Average and below-average values of Ca/Fe suggest that this was an interval of lower precipitation and weaker fluvial activity. Vegetation reflected reduction in the amounts of precipitation as the tropical forest declined, with species of Moraceae being the most affected tropical forest taxa. Climate conditions favored the diversity of dry tropical forest types. Fabaceae fluctuated, but values remained relatively high. Mangrove vegetation increased, although *Conocarpus erectus* was still the most representative mangrove species. *Rhizophora mangle* appeared almost continuously, and there were periods when *Avicennia germinans* and *Laguncularia racemosa* occurred. Temperate vegetation declined, although *Pinus sp*. appeared continuously with low values. Disturbance vegetation showed an increasing trend, but values fluctuated abruptly. Poaceae and Amaranthaceae were the best represented taxa, and continuous presence of Asteraceae, *Borreria sp*., *Zea mays* and Malvaceae suggest an increase in human activities in the region. The highly variable pollen types suggest different environments, dispersed regionally, a consequence of the coupled effect of increased ENSO activity and ITCZ migration (Joo-Chang et al., 2015) and frequent storm and hurricane activity (McCloskey and Keller, 2009).

Mangrove decreased abruptly around 3400 cal yr B.P. *Conocarpus erectus* almost disappeared and other mangrove taxa were absent. Fabaceae disappeared, but Moraceae increased along with Euphorbiaceae, *Brosimum alicastrum* and *Bursera simaruba*. Disturbance vegetation increased and temperate vegetation remained low. Although this period coincides with intense ENSO activity (Moy et al., 2002; Sandweiss et al., 2001), the increase of Moraceae and the presence of other taxa related to humid environments like *Pachira aquatica* refute the hypothesis that ENSO induced dryness. Nevertheless, this was an isolated episode and the chronological uncertainties made the comparison of punctual isolated episodes of vegetation change at decadal timescales impossible.

Geochemical data show a trend toward gradually decreasing precipitation and fluvial activity between ca. 3400 and 2600 cal yr B.P. The pollen record shows a general drying trend, with progressive reduction of mangrove vegetation and increasing disturbance vegetation. Nevertheless, tropical forest remained relatively stable with the dry tropical forest dominating the landscape over semi-evergreen tropical forest. Taxa of secondary vegetation show increased percentages, suggesting favorable conditions for herbaceous plant communities. Although ENSO activity was recorded during this period (Conroy et al., 2008; Moy et al., 2002), ENSO alone cannot explain successional changes, and shifts in ITCZ position (Haug et al., 2001, 2003) may, in part, explain changes in vegetation cover. Nevertheless, this period also coincided with low solar activity (Bond et al., 2001; van Geel et al., 2000) and the coupled effects of ENSO and ITCZ may explain the rapidly changing precipitation in the region.

Deposition of lowest amounts of Ca-bearing carbonates and/or highest abundance of Fe-bearing oxides and clays between ~2600 and ~2000 cal yr B.P. reflect the driest period in the Rio Hondo record. This interval is contemporary with arid conditions observed at the western margin (Los Petenes, Roy et al., 2017a), northern margin (Rio Lagartos; Aragón-Moreno et al., 2012) and in the central part (Lake Chichancanab; Hodell et al., 2005) of the peninsula. The driest period of the Rio Hondo record was registered at around 2600 cal yr B.P. Asteraceae reached its highest value and other disturbance taxa associated with agriculture and human activities, like Acacia-type and *Zea mays* (Torrescano-Valle and Islebe, 2015) appeared. Mangrove vegetation decreased and tropical forest decreased to its lowest values. Following this drying period, conditions were favorable for tropical forest and mangrove recovery, although precipitation remained relatively low in the Maya Lowlands (Hodell et al., 2001). Between ca. 2600 and 2100 cal yr B.P., mangrove vegetation increased. *Rhizophora mangle* appeared continuously and *Conocarpus erectus* fluctuated with high values. Moraceae increased and *Brosimum alicastrum* appeared continuously, suggesting semi-evergreen tropical forest cover increase. Fabaceae remained low and disturbance taxa like Poaceae and Amaranthaceae remained low. *Zea mays* was almost absent, and local agricultural activities may appear suppressed by increased regional pollen production. Taxa of temperate affinity maintained low values, suggesting continuous input of those taxa from savanna vegetation of the northern Belize. This period was previously reported to have been one of minor ENSO activity (Moy et al., 2002) and relatively stable ITCZ position (Haug et al., 2001; Medina-Elizalde et al., 2016).

Conditions became favorable again for tropical forest and mangrove expansion ca. 2100–1700 cal yr B.P. Precipitation increased relative to the interval of ca. 2600–2100 cal yr B.P. It is suggested by relatively higher, but below average Ca/Fe values, and this interval is contemporary with arid conditions at Los Petenes (Roy et al., 2017a), Río Lagartos (Aragón-Moreno et al., 2012) and Lake Tzib (Carrillo-Bastos et al., 2010). Disturbance elements declined, although the presence of Convolvulaceae and some records of *Zea mays* corroborate agriculture and human activities in the region during this time. Mangrove vegetation increased and appearance of *Rhizophora mangle* could be related to a change in sediment texture, from finer silty-clay to coarser medium and fine sand (e.g. Roy et al., 2017a). This period corresponds to the Late Preclassic and the beginning of the Classic Maya periods, when climatic conditions were favorable. Lachniet et al. (2017) showed that the last two millennia have been highly variable in terms of ENSO activity and NAO variability, with periods of northern ITCZ position and others of drought related to intensified ENSO activity. Although geochemical data suggest increasing precipitation, taxa associated with dry tropical forest dominate over semi-evergreen tropical forest in the pollen spectra, which could be related to highly variable ENSO activity that favored species like *Haematoxylum campechianum*, *Caesalpinia sp*., *Pithecellobium sp*., *Bursera simaruba* and some taxa of the Sapotaceae. These taxa, however, occur in different tropical forest types and have high tolerance to changes in precipitation.

5.2. Palaeoclimatic forcing

Despite some chronological uncertainty, the comparisons between geochemistry/pollen and other climate proxies in the Caribbean region and eastern Pacific corroborate the sensitivity of the site to external climate drivers during the middle and late Holocene (Fig. 6). Several authors have shown that the middle Holocene was relatively stable in the Caribbean region (Haug et al., 2001; Hodell et al., 1991; Lachniet et al., 2004; Mueller et al., 2009; Pollock et al., 2016), but particularly wet (Lachniet et al., 2004; Metcalfe et al., 2009) with more precipitation (Pollock et al., 2016) and cooler SSTs than present (Giry et al., 2012). This climate configuration could modulate ENSO activity, given the northern position of the ITCZ (Koutavas et al., 2006). Nevertheless, the transition from the middle to late Holocene occurred abruptly (Magny and Haas, 2004; Mayewski et al., 2004; Wanner et al., 2008). Wahl et al. (2014) showed that climate in southern Maya Lowlands, located at the western portion of the Caribbean sea, was influenced more by changes in Tropical Atlantic climate during the middle

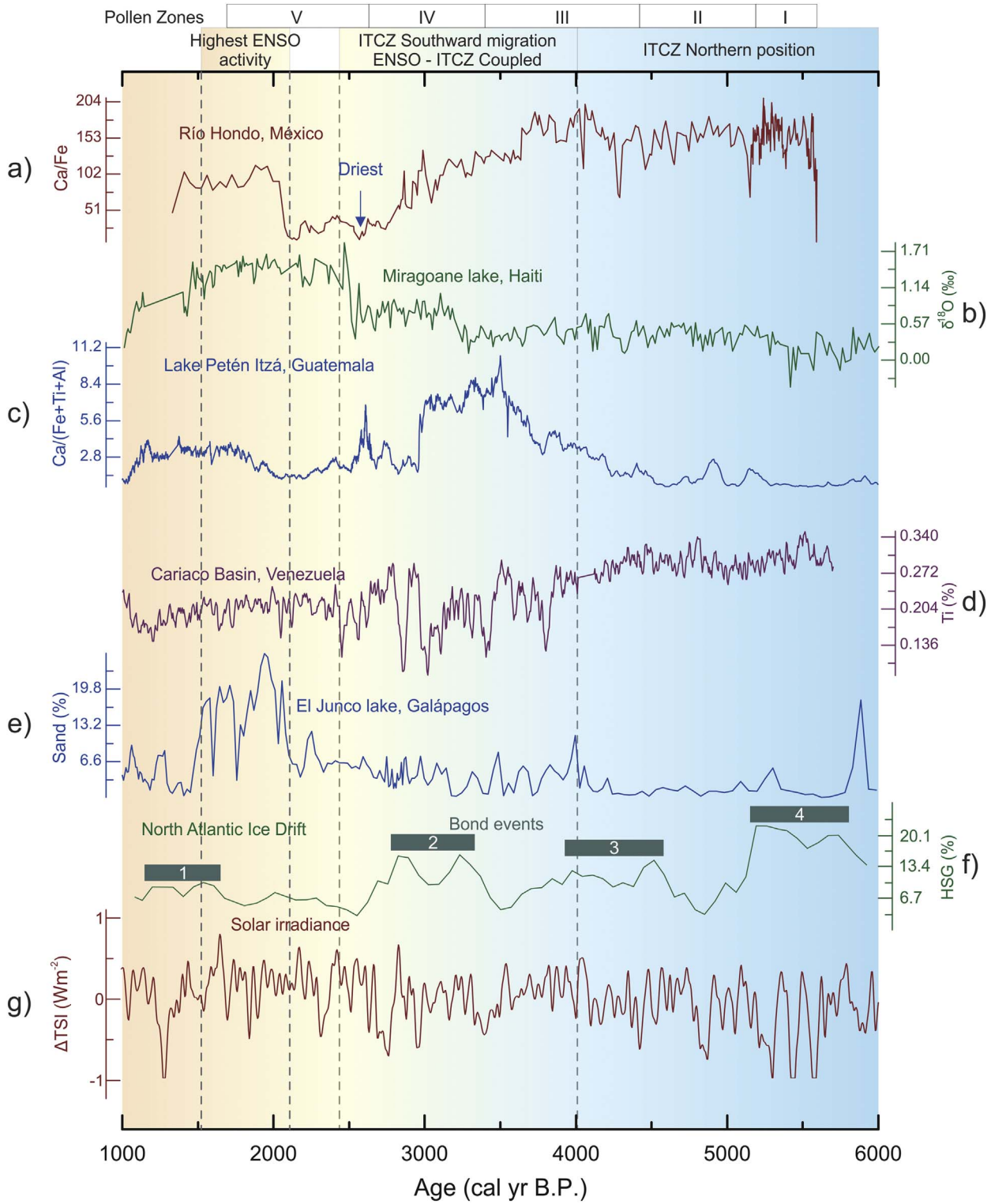

Fig. 6. Comparison of Rio Hondo geochemical data with other Atlantic and Eastern Pacific studies, (a) Runoff variation at Río Hondo, (b) Lake level variability through changes oxygen isotopes ratio at Lake Miragoane, Haiti (Hodell et al., 1991), (c) Precipitation changes at Lake Petén Itzá, Guatemala (Mueller et al., 2009), (d) Cariaco basin precipitations (Haug et al., 2001), (e) ENSO indicator at El Junco Lake, Galapagos (Conroy et al., 2008), (f) Hemalite Stained Grains as Drift Ice Index with Bond events 1 to 4 indicated by color bars (Bond et al., 2001), (g) Total solar irradiance (Steinhilber et al., 2009).

Holocene, until ~3.8 kyr B.P., when increasing ENSO activity became strong enough to affect western Caribbean climate. Our geochemical data is in agreement with their interpretations; Rio Hondo appears not to have been very sensitive to enhanced ENSO activity before ~4 kyr B.P., although data show isolated episodes of reduced precipitation between 5.6 and 4 kyr B.P. that can be related to cooler global conditions (Lachniet et al., 2004) and climate overturning during the middle to late Holocene (Magny and Haas, 2004) by means of ENSO activity (Conroy et al., 2008; Rein et al., 2005), cooling episodes (Bond et al., 2001) and southward migration of the ITCZ (Bernal et al., 2011; Wang et al., 2005).

Despite these episodes of abrupt shifts in precipitation, Rio Hondo

precipitation remained sufficiently high to support high sedimentation rates. This is in agreement with other inferences for higher precipitation in the Caribbean region (Haug et al., 2001; Pollock et al., 2016) and in nearby cores taken in Belize (Wooller et al., 2004, 2007) during the middle Holocene, until around 4.0 kyr B.P. At that time, Ca/Fe ratios started to decrease along with increased ENSO activity (Fig. 6), as detected in marine (Conroy et al., 2008; Rein et al., 2005) and continental records (Moy et al., 2002). Staubwasser et al. (2003) described a severe dry period centered at ca. 4.2 kyr B.P. in South Asia related to changes in solar irradiance. Mayewski et al. (2004) classified this epoch (4.2–3.8 kyr B.P.) as a period of rapid climate change, although signals and intensities differ among records. Booth et al. (2005) described a North American megadrought between 4.3 and 4.1 kyr B.P. as a result of changes in global climate. Although they discard North Atlantic climate dynamics as a causal mechanism, they recognized the lack of information to assess the role of external forcings like solar variability or increased volcanism. Finally, Fisher et al. (2008) associated this period with the onset of the modern ENSO configuration. Our record shows two episodes of dryness, at ~4.3 and ~4.0 kyr B.P., which can be related to global climate change episodes and the formal end of the middle Holocene (Walker et al., 2012). Following these global climate events, the southward migration of the ITCZ reduced precipitation in the Caribbean region (Haug et al., 2001), the Asian monsoon diminished in strength (Staubwasser et al., 2003), the African tropics entered a period of severe drought (Thompson et al., 2002), and ENSO activity intensified (Moy et al., 2002).

Carrillo-Bastos et al. (2013) reconstructed quantitatively the precipitation on the northern Yucatán Peninsula over the last 4000 years. Although their calculations were based on a different location, the oldest part of the record suggests that precipitation was almost 7% higher than present. Therefore, considering the time window of the study, the Rio Hondo location and evidence of earlier wetter-than-present conditions in the Caribbean, precipitation could have been > 10% higher than present prior to 4.2 kyr B.P. A highly variable period, however, was registered between 3.0 and 2.8 kyr B.P. that can be related to low solar activity (Bond et al., 2001; van Geel et al., 2000) (Fig. 6). Several authors have discussed this climate anomaly (Berrío et al., 2006; Blaauw et al., 2004; Mayewski et al., 2004; van Geel et al., 1996, 2000), but the timing differs among records. Haug et al. (2001) suggested tradewind-driven upwelling as a probable explanation for Cariaco Basin's metal (Ti and Fe) fluctuations during this period, but this explanation may not apply to the Rio Hondo record, given that the sampling site is protected from the Trade Winds and has a very shallow water column. Moreover, the Lake Peten Itza record, from northern Guatemala (Mueller et al., 2009), shows anomalous behavior in the geochemical record as well. This period is characterized by the coupled effect of strong ENSO events and highly variable ITCZ position (Joo-Chang et al., 2015; Toth et al., 2012). At ~2.6 kyr B.P., a severe drought was registered in multiple records from the region, and marked the period of human occupation (Akers et al., 2016; Webster et al., 2007a, 2007b). Rio Hondo's geochemical data show the end of a prolonged drying period and reduction of ENSO activity at 2.5 kyr B.P. Precipitation remained low with some episodes of increased humidity until ~2.0 kyr B.P. Climate in the last two millennia differs from climate in previous periods; ENSO activity between 2 and 1.3 kyr B.P. presents the highest frequency of the entire Holocene, although its effect on the Caribbean region are not clear. Rio Hondo recorded abrupt changes in precipitation during this time. This interval was previously reported in southwestern Mexico and the southern Caribbean (Velez et al., 2014), with intensified ENSO activity (Conroy et al., 2008; Moy et al., 2002) and a northern ITCZ position (Lachniet et al., 2017). The Cariaco Basin record received less precipitation, whereas rainfall increased in the Rio Hondo. In this regard, Jury et al. (2007) demonstrated that ENSO events, which are generated in the central Pacific (ENSO 3.4), may increase Caribbean precipitation, except in the southeastern region, which could explain its absence in Cariaco Basin's record.

6. Conclusions

A sediment core from the Rio Hondo Delta, provides evidence for changes in precipitation and vegetation in the southeastern Mexico and the northwestern Caribbean during the middle and late Holocene. Climate in the region during the middle Holocene was more influenced by the forcings associated with Atlantic climate dynamics, and greater precipitation that favored semi-evergreen tropical forest. Nevertheless, at the end of the middle Holocene, climate and vegetation were strongly influenced by ENSO activity. The beginning of the late Holocene was characterized by a dynamic ITCZ and dry conditions.

Local and regional vegetation responded to major global climate events at 5200 cal yr B.P., 4200 and 2600 cal yr B.P. These major climate events were observed, with a short lag time, despite the multi-decadal resolution of the pollen samples. Vegetation response to major climate forcings like ENSO, NAO and ITCZ were clearly reflected by pollen spectra. Vegetation responded to changes in atmospheric patterns that operate at different timescales whereby latitudinal shifts in the position of the ITCZ altered vegetation by changing the distribution of humidity, and ENSO importance increased during the late Holocene, resulting in greater dominance of dry tropical forests.

Both semi-evergreen tropical forest and dry tropical forest expansion were recorded. The drying trend peaked around 2600 cal yr B.P. (the driest period in the Rio Hondo record) and climate stabilized and tropical forest started to recover until ca. 2000 cal yr B.P. when ENSO activity was intense. This drove tropical forest expansion as well, although the pollen record indicates that different tropical forest types prevailed as a response to intensified ENSO variability.

Disturbance taxa associated to human activities and agriculture persisted the entire sediment archive, nevertheless mangroves and tropical forest respond to major climate forcings. These findings suggest that human activities did not influence climatic changes alone and more research is needed to determine the role of Maya culture development in regional climate evolution during middle and late Holocene.

Geochemical and palaeoecological data reflect changes in global and regional climate change under specific time scales. Nevertheless, it is expected that chronology of reconstructed climate events might have inherented uncertainty from decadal to centennial time-scale due to variations in sedimentation rate associated with limited numbers of radiocarbon dates. Finally, further research has to be made in order to reduce chronological uncertainties and to incorporate a quantitative approach to determine the possible cycles and temporality of main major drivers of climate in the Yucatan Peninsula.

Acknowledgments

Conacyt (127613) is acknowledged for funding the project Variabilidad climática y paleoecología de los últimos 1500 años del sureste de México. PDR received PASPA scholarship from DGAPA-UNAM for a sabbatical at ECOSUR. Dr. Mark Brenner, Dr. Matthew Wooller and one anonymous reviewer made helpful comments on an earlier version of this manuscript.

References

Akers, P.D., Brook, G.A., Railsback, L.B., Liang, F., Iannone, G., Webster, J.W., Reeder, P.P., Cheng, H., Edwards, R.L., 2016. An extended and higher-resolution record of climate and land use from stalagmite MC01 from Macal Chasm, Belize, revealing connections between major dry events, overall climate variability, and Maya socio-political changes. Palaeogeogr. Palaeoclimatol. Palaeoecol. 459, 268–288.

Anselmetti, F.S., Hodell, D.A., Ariztegui, D., Brenner, M., Rosenmeier, M.F., 2007. Quantification of soil erosion rates related to ancient Maya deforestation. Geology 35, 915–918.

Aragón-Moreno, A.A., Islebe, G.A., Torrescano-Valle, N., 2012. A ~3800-yr, high-resolution record of vegetation and climate change on the north coast of the Yucatan Peninsula. Rev. Palaeobot. Palynol. 178, 35–42.

Baker, J.L., Lachniet, M.S., Chervyatsova, O., Asmerom, Y., Polyak, V.J., 2017. Holocene warming in western continental Eurasia driven by glacial retreat and greenhouse forcing. Nat. Geosci. 10, 430–435.

Bates, C.D., Coxon, P., Gibbard, P.L., 1978. A new method for the preparation of clay-rich sediment samples for palynological investigation. New Phytol. 81, 459–463.
Beach, T., Luzzadder-Beach, S., Dunning, N., Cook, D., 2008. Human and natural impacts on fluvial and karst depressions of the Maya Lowlands. Geomorphology 101, 308–331.
Bernal, J.P., Lachniet, M., McCulloch, M., Mortimer, G., Morales, P., Cienfuegos, E., 2011. A speleothem record of Holocene climate variability from southwestern Mexico. Quat. Res. 75, 104–113.
Berrío, J.C., Hooghiemstra, H., Van Geel, B., Ludlow-Wiechers, B., 2006. Environmental history of the dry forest biome of Guerrero, Mexico, and human impact during the last c. 2700 years. The Holocene 16, 63–80.
Blaauw, M., van Geel, B., van der Plicht, J., 2004. Solar forcing of climatic change during the mid-Holocene: indications from raised bogs in The Netherlands. The Holocene 14, 35–44.
Bond, G., Kromer, B., Beer, J., Muscheler, R., Evans, M.N., Showers, W., Hoffmann, S., Lotti-Bond, R., Hajdas, I., Bonani, G., 2001. Persistent solar influence on North Atlantic climate during the Holocene. Science 294, 2130–2136.
Booth, R.K., Jackson, S.T., Forman, S.L., Kutzbach, J.E., Bettis, E.A., Kreigs, J., Wright, D.K., 2005. A severe centennial-scale drought in midcontinental North America 4200 years ago and apparent global linkages. The Holocene 15, 321–328.
Bridgewater, S., Ibanez, A., Ratter, J.A., Furley, P., 2002. Vegetation classification and floristics of the savannas and associated wetlands of the Rio Bravo Conservation and Management Area, Belize. Edinb. J. Bot. 59, 421–442.
Budowski, G., 1966. Los Bosques de los Trópicos Húmedos de América. Turrialba. 16. pp. 278–285.
Carrillo-Bastos, A., Islebe, G.A., Torrescano-Valle, N., González, N.E., 2010. Holocene vegetation and climate history of central Quintana Roo, Yucatán Península, Mexico. Rev. Palaeobot. Palynol. 160, 189–196.
Carrillo-Bastos, A., Islebe, G.A., Torrescano-Valle, N., 2013. 3800 years of quantitative precipitation reconstruction from the Northwest Yucatan Peninsula. PLoS One 8, e84333.
Chauhan, B.S., Johnson, D.E., 2008. Seed germination ecology of purple-leaf button weed (*Borreria ocymoides*) and Indian heliotrope (*Heliotropium indicum*): two common weeds of rain-fed rice. Weed Sci. 56, 670–675.
Conroy, J.L., Overpeck, J.T., Cole, J.E., Shanahan, T.M., Steinitz-Kannan, M., 2008. Holocene changes in eastern tropical Pacific climate inferred from a Galápagos lake sediment record. Quat. Sci. Rev. 27, 1166–1180.
Curtis, J.H., Hodell, D.A., Brenner, M., 1996. Climate variability on the Yucatan Peninsula (Mexico) during the past 3500 years, and implications for Maya cultural evolution. Quat. Res. 46, 37–47.
deMenocal, P., Ortiz, J., Guilderson, T., Adkins, J., Sarnthein, M., Baker, L., Yarusinsky, M., 2000. Abrupt onset and termination of the African Humid Period: rapid climate responses to gradual insolation forcing. Quat. Sci. Rev. 19, 347–361.
Faegri, K., Iversen, J., 1989. Textbook of Pollen Analysis, 4th ed. John Wiley.
Fisher, D., Osterberg, E., Dyke, A., Dahl-Jensen, D., Demuth, M., Zdanowicz, C., Bourgeois, J., Koerner, R.M., Mayewski, P., Wake, C., Kreutz, K., Steig, E., Zheng, J., Yalcin, K., Goto-Azuma, K., Luckman, B., Rupper, S., 2008. The Mt Logan Holocene—late Wisconsinan isotope record: tropical Pacific—Yukon connections. The Holocene. http://dx.doi.org/10.1177/0959683608092236.
Ford, A., 2008. Dominant plants of the Maya forest and gardens of El Pilar: implications for paleoenvironmental reconstructions. J. Ethnobiol. 28, 179–199.
Ford, A., Nigh, R., 2009. Origins of the Maya forest garden: Maya resource management. J. Ethnobiol. 29, 213–236.
Gill, R.B., 2001. The Great Maya Droughts: Water, Life, and Death. University of New Mexico Press.
Giry, C., Felis, T., Kölling, M., Scholz, D., Wei, W., Lohmann, G., Scheffers, S., 2012. Mid- to late Holocene changes in tropical Atlantic temperature seasonality and interannual to multidecadal variability documented in southern Caribbean corals. Earth Planet. Sci. Lett. 331–332, 187–200.
Giry, C., Felis, T., Koelling, M., Wei, W., Lohmann, G., Scheffers, S., 2013. Controls of Caribbean surface hydrology during the mid-to late Holocene: insights from monthly resolved coral records. Clim. Past 9, 841–858.
Gray, L.J., Beer, J., Geller, M., Haigh, J.D., Lockwood, M., Matthes, K., Cubasch, U., Fleitmann, D., Harrison, G., Hood, L., Luterbacher, J., Meehl, G.A., Shindell, D., van Geel, B., White, W., 2010. Solar influences on climate. Rev. Geophys. 48, RG4001.
Grimm, E.C., 1987. CONISS: a FORTRAN 77 program for stratigraphically constrained cluster analysis by the method of incremental sum of squares. Comput. Geosci. 13, 13–35.
Grimm, E.C., 2016. TILIA.
Haug, G.H., Hughen, K.A., Sigman, D.M., Peterson, L.C., Röhl, U., 2001. Southward migration of the intertropical convergence zone through the Holocene. Science 293, 1304–1308.
Haug, G.H., Günther, D., Peterson, L.C., Sigman, D.M., Hughen, K.A., Aeschlimann, B., 2003. Climate and the collapse of Maya civilization. Science 299, 1731–1735.
Hodell, D.A., Curtis, J.H., Jones, G.A., Higuera-Gundy, A., Brenner, M., Binford, M.W., Dorsey, K.T., 1991. Reconstruction of Caribbean climate change over the past 10, 500 years. Nature 352, 790–793.
Hodell, D.A., Brenner, M., Curtis, J.H., Guilderson, T., 2001. Solar forcing of drought frequency in the Maya lowlands. Science 292, 1367–1370.
Hodell, D.A., Brenner, M., Curtis, J.H., 2005. Terminal classic drought in the northern Maya lowlands inferred from multiple sediment cores in Lake Chichancanab (Mexico). Quat. Sci. Rev. 24, 1413–1427.
Hodell, D.A., Brenner, M., Curtis, J.H., 2007. Climate and cultural history of the north-eastern Yucatan Peninsula, Quintana Roo, Mexico. Clim. Chang. 83, 215–240.
Islebe, G.A., Hooghiemstra, H., Brenner, M., Curtis, J.H., Hodell, D.A., 1996. A Holocene vegetation history from lowland Guatemala. The Holocene 6, 265–271.
Islebe, G.A., Sánchez-Sánchez, O., Valdéz-Hernández, M., Weissenberger, H., 2015a. Distribution of vegetation types. In: Islebe, G.A., Calmé, S., León-Cortés, J.L., Schmook, B. (Eds.), Biodiversity and Conservation of the Yucatán Peninsula. Springer International Publishing, pp. 39–53.
Islebe, G.A., Schmook, B., Calmé, S., León-Cortés, J.L., 2015b. Introduction: biodiversity and conservation of the Yucatán Peninsula, Mexico. In: Islebe, G.A., Calmé, S., León-Cortés, J.L., Schmook, B. (Eds.), Biodiversity and Conservation of the Yucatán Peninsula. Springer International Publishing, pp. 1–5.
Jennerjahn, T.C., Ittekkot, V., Arz, H.W., Behling, H., Pätzold, J., Wefer, G., 2004. Asynchronous terrestrial and marine signals of climate change during Heinrich events. Science 306, 2236–2239.
Joo-Chang, J.C., Islebe, G.A., Torrescano-Valle, N., 2015. Mangrove history during middle-and late-Holocene in Pacific south-eastern Mexico. The Holocene 25 (4), 651–662.
Jury, M., Malmgren, B.A., Winter, A., 2007. Subregional precipitation climate of the Caribbean and relationships with ENSO and NAO. J. Geophys. Res. 112, D16107.
Khan, N.S., Ashe, E., Horton, B.P., Dutton, A., Kopp, R.E., 2017. Drivers of Holocene sea-level change in the Caribbean. Quat. Sci. Rev. 155, 13–36.
Klotzbach, P.J., 2011. The influence of El Nino-southern oscillation and the Atlantic multidecadal oscillation on Caribbean tropical cyclone activity. J. Clim. 24, 721–731.
Koutavas, A., deMenocal, P.B., Olive, G.C., Lynch-Stieglitz, J., 2006. Mid-Holocene El Niño–Southern Oscillation (ENSO) attenuation revealed by individual foraminifera in eastern tropical Pacific sediments. Geology 34, 993–996.
Kovacs, S.E., Reinhardt, E.G., Chatters, J.C., Rissolo, D., Schwarcz, H.P., Collins, S.V., Kim, S.-T., Nava Blank, A., Luna Erreguerena, P., 2017. Calcite raft geochemistry as a hydrological proxy for Holocene aquifer conditions in Hoyo Negro and Ich Balam (Sac Actun Cave System), Quintana Roo, Mexico. Quat. Sci. Rev. 175, 97–111.
Lachniet, M.S., Asmerom, Y., Burns, S.J., Patterson, W.P., Polyak, V.J., Seltzer, G.O., 2004. Tropical response to the 8200 yr B.P. cold event? Speleothem isotopes indicate a weakened early Holocene monsoon in Costa Rica. Geology 32, 957–960.
Lachniet, M.S., Asmerom, Y., Polyak, V., Bernal, J.P., 2017. Two millennia of Mesoamerican monsoon variability driven by Pacific and Atlantic synergistic forcing. Quat. Sci. Rev. 155, 100–113.
Lentz, D.L., Dunning, N.P., Scarborough, V.L., Magee, K.S., Thompson, K.M., Weaver, E., Carr, C., Terry, R.E., Islebe, G., Tankersley, K.B., Grazioso Sierra, L., Jones, J.G., Buttles, P., Valdez, F., Ramos Hernandez, C.E., 2014. Forests, fields, and the edge of sustainability at the ancient Maya city of Tikal. Proc. Natl. Acad. Sci. U. S. A. 111, 18513–18518.
Magny, M., Haas, J.N., 2004. A major widespread climatic change around 5300 cal. yr BP at the time of the Alpine Iceman. J. Quat. Sci. 19, 423–430.
Mayewski, P.A., Rohling, E.E., Curt Stager, J., Karlén, W., Maasch, K.A., David Meeker, L., Meyerson, E.A., Gasse, F., van Kreveld, S., Holmgren, K., Lee-Thorp, J., Rosqvist, G., Rack, F., Staubwasser, M., Schneider, R.R., Steig, E.J., 2004. Holocene climate variability. Quat. Res. 62, 243–255.
McCloskey, T.A., Keller, G., 2009. 5000 year sedimentary record of hurricane strikes on the central coast of Belize. Quat. Int. 195, 53–68.
Medina-Elizalde, M., Burns, S.J., Polanco-Martínez, J.M., Beach, T., Lases-Hernández, F., Shen, C.-C., Wang, H.-C., 2016. High-resolution speleothem record of precipitation from the Yucatan Peninsula spanning the Maya Preclassic Period. Glob. Planet. Chang. 138, 93–102.
Metcalfe, S., Breen, A., Murray, M., Furley, P., Fallick, A., McKenzie, A., 2009. Environmental change in northern Belize since the latest Pleistocene. J. Quat. Sci. 24, 627–641.
Metcalfe, S.E., Barron, J.A., Davies, S.J., 2015. The Holocene history of the north American monsoon: "known knowns" and "known unknowns" in understanding its spatial and temporal complexity. Quat. Sci. Rev. 120, 1–27.
Moreno-Casasola, P., Espejel, I., 1986. Classification and ordination of coastal sand dune vegetation along the Gulf and Caribbean Sea of Mexico. Vegetatio 66, 147–182.
Moy, C.M., Seltzer, G.O., Rodbell, D.T., Anderson, D.M., 2002. Variability of El Niño/Southern Oscillation activity at millennial timescales during the Holocene epoch. Nature 420, 162–165.
Mueller, A.D., Islebe, G.A., Hillesheim, M.B., Grzesik, D.A., Anselmetti, F.S., Ariztegui, D., Brenner, M., Curtis, J.H., Hodell, D.A., Venz, K.A., 2009. Climate drying and associated forest decline in the lowlands of northern Guatemala during the late Holocene. Quat. Res. 71, 133–141.
Muñoz, E., Busalacchi, A.J., Nigam, S., Ruiz-Barradas, A., 2008. Winter and summer structure of the Caribbean low-level jet. J. Clim. 21, 1260–1276.
Muñoz, P., Gorin, G., Parra, N., Velásquez, C., Lemus, D., Monsalve, M.C., Jojoa, M., 2017. Holocene climatic variations in the western Cordillera of Colombia: a multi-proxy high-resolution record unravels the dual influence of ENSO and ITCZ. Quat. Sci. Rev. 155, 159–178.
Nakagawa, T., Brugiapaglia, E., Digerfeldt, G., Reille, M., Beaulieu, J.-L.D.E., Yasuda, Y., 1998. Dense-media separation as a more efficient pollen extraction method for use with organic sediment/deposit samples: comparison with the conventional method. Boreas 27, 15–24.
Orellana, R., Islebe, G., Espadas, C., 2003. Presente, pasado y futuro de los climas de la Península de Yucatán. In: Colunga-GarcíaMarín, P., Larqué-Saavedra, A. (Eds.), Naturaleza Y Sociedad En El Área Maya: Pasado, Presente Y Futuro. Academia Mexicana de Ciencias/Centro de Investigación Científica de Yucatán, Mérida, pp. 37–52.
Palacios-Chávez, R., Ludlow-Wiechers, B., Villanueva, G.R., 1991. Flora palinológica de la reserva de la biosfera de Sian Ka'an, Quintana Roo, México. Centro de Investigaciones de Quintana Roo.
Pohl, M.D., Pope, K.O., Jones, J.G., Jacob, J.S., Piperno, D.R., deFrance, S.D., Lentz, D.L., Gifford, J.A., Danforth, M.E., Josserand, J.K., 1996. Early agriculture in the Maya lowlands. Lat. Am. Antiq. 7, 355–372.

Pollock, A.L., van Beynen, P.E., DeLong, K.L., Polyak, V., Asmerom, Y., Reeder, P.P., 2016. A mid-Holocene paleoprecipitation record from Belize. Palaeogeogr. Palaeoclimatol. Palaeoecol. 463, 103–111.
Reimer, P.J., Bard, E., Bayliss, A., Warren Beck, J., Blackwell, P.G., Ramsey, C.B., Buck, C.E., Cheng, H., Lawrence Edwards, R., Friedrich, M., Grootes, P.M., Guilderson, T.P., Haflidason, H., Hajdas, I., Hatté, C., Heaton, T.J., Hoffmann, D.L., Hogg, A.G., Hughen, K.A., Felix Kaiser, K., Kromer, B., Manning, S.W., Niu, M., Reimer, R.W., Richards, D.A., Marian Scott, E., Southon, J.R., Staff, R.A, Turney, C.S.M., van der Plicht, J., 2013. IntCal13 and Marine13 radiocarbon age calibration curves 0–50,000 years cal BP. Radiocarbon 55, 1869–1887.
Rein, B., Lückge, A., Reinhardt, L., Sirocko, F., Wolf, A., Dullo, W.-C., 2005. El Niño variability off Peru during the last 20,000 years. Paleoceanography 20, PA4003.
Rollins, H.B., Richardson, J.B., Sandweiss, D.H., 1986. The birth of El Niño: geoarchaeological evidence and implications. Geoarchaeology 1, 3–15.
Rosenmeier, M.F., Hodell, D.A., Brenner, M., Curtis, J.H., Guilderson, T.P., 2002. A 4000-year lacustrine record of environmental change in the southern Maya Lowlands, Petén, Guatemala. Quat. Res. 57, 183–190.
Roy, P.D., Torrescano-Valle, N., Islebe, G.A., Gutiérrez-Ayala, L.V., 2017a. Late Holocene hidroclimate of the western Yucatan Peninsula (Mexico). J. Quat. Sci. http://dx.doi.org/10.1002/jqs.2988.
Roy, P.D., Torrescano-Valle, N., Escarraga-Paredes, D. del S., Vela-Pelaez, A.A., Lozano-Santacruz, R., 2017b. Comparison of elemental concentration in surface sediments and precipitation regimes of the Yucatán Peninsula, México. Bol. Geol. Min.
Russell, J., Talbot, M.R., Haskell, B.J., 2003. Mid-holocene climate change in Lake Bosumtwi, Ghana. Quat. Res. 60, 133–141.
Sánchez-Sánchez, O., Islebe, G.A., 2002. Tropical forest communities in southeastern Mexico. Plant Ecol. 158, 183–200.
Sandweiss, D.H., Richardson, J.B., Reitz, E.J., Rollins, H.B., Maasch, K.A., 1996. Geoarchaeological evidence from Peru for a 5000 years B.P. onset of El Nino. Science 273, 1531–1533.
Sandweiss, D.H., Maasch, K.A., Burger, R.L., Richardson, J.B., Rollins, H.B., Clement, A., 2001. Variation in Holocene El Niño frequencies: climate records and cultural consequences in ancient Peru. Geology 29, 603–606.
Staubwasser, M., Sirocko, F., Grootes, P.M., Segl, M., 2003. Climate change at the 4.2 ka BP termination of the Indus valley civilization and Holocene south Asian monsoon variability. Geophys. Res. Lett. 30 (1425).
Steinhilber, F., Beer, J., Fröhlich, C., 2009. Total solar irradiance during the Holocene. Geophys. Res. Lett. 36, L19704.
Stuiver, M., Reimer, P.J., Reimer, R.W., 2017. CALIB 7.1 [WWW Document]. CALIB 7.1 [WWW program]. http://calib.org/calib/ (accessed 3.30.17).
Thompson, L.G., Mosley-Thompson, E., Davis, M.E., Henderson, K.A., Brecher, H.H., Zagorodnov, V.S., Mashiotta, T.A., Lin, P.-N., Mikhalenko, V.N., Hardy, D.R., Beer, J., 2002. Kilimanjaro ice core records: evidence of holocene climate change in tropical Africa. Science 298, 589–593.
Thompson, L.G., Mosley-Thompson, E., Brecher, H., Davis, M., León, B., Les, D., Lin, P.-N., Mashiotta, T., Mountain, K., 2006. Abrupt tropical climate change: past and present. Proc. Natl. Acad. Sci. U. S. A. 103, 10536–10543.
Torrescano-Valle, N., Folan, W.J., 2015. Physical settings, environmental history, with and outlook on global change. In: Islebe, G.A., Calmé, S., León-Cortés, J.L., Schmook, B. (Eds.), Biodiversity and Conservation of the Yucatán Peninsula. Springer International Publishing, pp. 9–37.
Torrescano-Valle, N., Islebe, G.A., 2006. Tropical forest and mangrove history from southeastern Mexico: a 5000 yr pollen record and implications for sea level rise. Veg. Hist. Archaeobotany 15, 191–195.
Torrescano-Valle, N., Islebe, G.A., 2015. Holocene paleoecology, climate history and human influence in the southwestern Yucatán Peninsula. Rev. Palaeobot. Palynol. 217, 1–8.
Toscano, M.A., Macintyre, I.G., 2003. Corrected western Atlantic sea-level curve for the last 11,000 years based on calibrated 14C dates from *Acropora palmata* framework and intertidal mangrove peat. Coral Reefs 22, 257–270.
Toth, L.T., Aronson, R.B., Vollmer, S.V., Hobbs, J.W., Urrego, D.H., Cheng, H., Enochs, I.C., Combosch, D.J., van Woesik, R., Macintyre, I.G., 2012. ENSO drove 2500-year collapse of eastern Pacific coral reefs. Science 337, 81–84.
Tovilla-Hernández, C., Orihuela-Belmonte, D.E., Salas-Tobledo, R.L., 2009. Estructura, composición, regeneración y extracción de madera de los bosques de manglar. In: Espinosa-Avalos, J., Islebe, G.A., Hernández-Arana, H.A. (Eds.), El Sistema Ecológico de La Bahía de Chetumal/Corozal: Costa Occidental Del Mar Caribe. El Colegio de la Frontera Sur, pp. 45–60.
van Geel, B., Buurman, J., Waterbolk, H.T., 1996. Archaeological and palaeoecological indications of an abrupt climate change in The Netherlands, and evidence for climatological teleconnections around 2650 BP. J. Quat. Sci. 11, 451–460.
van Geel, B., Heusser, C.J., Renssen, H., Schuurmans, C.J.E., 2000. Climatic change in Chile at around 2700 BP and global evidence for solar forcing: a hypothesis. The Holocene 10, 659–664.
Velez, M.I., Escobar, J., Brenner, M., Rangel, O., Betancourt, A., Jaramillo, A.J., Curtis, J.H., Moreno, J.L., 2014. Middle to late Holocene relative sea level rise, climate variability and environmental change along the Colombian Caribbean coast. The Holocene 24, 898–907.
Wahl, D., Byrne, R., Anderson, L., 2014. An 8700 year paleoclimate reconstruction from the southern Maya lowlands. Quat. Sci. Rev. 103, 19–25.
Walker, M.J.C., Berkelhammer, M., Björck, S., Cwynar, L.C., Fisher, D.A., Long, A.J., Lowe, J.J., Newnham, R.M., Rasmussen, S.O., Weiss, H., 2012. Formal subdivision of the Holocene series/epoch: a discussion paper by a working group of INTIMATE (integration of ice-core, marine and terrestrial records) and the subcommission on quaternary stratigraphy (International Commission on Stratigraphy). J. Quat. Sci. 27, 649–659.
Wang, Y., Cheng, H., Edwards, R.L., He, Y., Kong, X., An, Z., Wu, J., Kelly, M.J., Dykoski, C.A., Li, X., 2005. The Holocene Asian monsoon: links to solar changes and North Atlantic climate. Science 308, 854–857.
Wanner, H., Beer, J., Bütikofer, J., Crowley, T.J., Cubasch, U., Flückiger, J., Goosse, H., Grosjean, M., Joos, F., Kaplan, J.O., Küttel, M., Müller, S.A., Prentice, I.C., Solomina, O., Stocker, T.F., Tarasov, P., Wagner, M., Widmann, M., 2008. Mid- to late Holocene climate change: an overview. Quat. Sci. Rev. 27, 1791–1828.
Webster, J.W., Brook, G.A., Railsback, L.B., Cheng, H., Edwards, R.L., Alexander, C., Reeder, P.P., 2007a. Stalagmite evidence from Belize indicating significant droughts at the time of Preclassic abandonment, the Maya hiatus, and the classic Maya collapse. Palaeogeogr. Palaeoclimatol. Palaeoecol. 250, 1–17.
Webster, J.W., Brook, G.A., Railsback, L.B., Cheng, H., Edwards, R.L., Alexander, C., Reeder, P.P., 2007b. Stalagmite evidence from Belize indicating significant droughts at the time of Preclassic abandonment, the Maya hiatus, and the classic Maya collapse. Palaeogeogr. Palaeoclimatol. Palaeoecol. 250, 1–17.
Wooller, M.J., Behling, H., Smallwood, B.J., Fogel, M., 2004. Mangrove ecosystem dynamics and elemental cycling at Twin Cays, Belize, during the Holocene. J. Quat. Sci. 19, 703–711.
Wooller, M.J., Morgan, R., Fowell, S., Behling, H., Fogel, M., 2007. A multiproxy peat record of Holocene mangrove palaeoecology from Twin Cays, Belize. The Holocene 17, 1129–1139.
Yao, Q., Liu, K.-B., 2017. Dynamics of marsh-mangrove ecotone since the mid-Holocene: a palynological study of mangrove encroachment and sea level rise in the Shark River Estuary, Florida. PLoS One 12, e0173670.